

Variation of N_{\parallel} and its Effect on Fast Wave Electron Heating on LHD

TAKEUCHI Norio, SEKI Tetsuo¹, TORII Yuki, SAITO Kenji¹, WATARI Tetsuo¹,
TAKASE Yuichi², KUMAZAWA Ryuhei¹, MUTOH Takashi¹, WATANABE Tsuguhiro¹
and ZHAO Yanping³

Nagoya University, Nagoya 464-8603, Japan

¹*National Institute for Fusion Science, Toki 509-5292, Japan*

²*Tokyo University, Kashiwa 277-8562 Japan*

³*Institute of Plasma Physics, Academia Sinica, Hefei 230031, P.R. China*

(Received: 9 December 2003 / Accepted: 5 August 2004)

Abstract

It is predicted in a theory that the MHD stability of LHD plasma depends strongly on the profile of rotational transform, suggesting that the performance of the plasma is improved by controlling it. In order to control the profile, we have proposed a comblin antenna for the ICRF fast wave current drive. The propagation and absorption of the wave excited by this antenna is studied in this paper by use of ray tracing analysis. It is concluded that the strong electron heating occurs when the frequency and wave number are adequately chosen. It is also found that up-shift of parallel wave number occurs as the ray travels and the wave absorption is enhanced. The same calculation is carried out in the tokamak with the similar size and plasma parameters, and it is found that the k_{\parallel} -shift in the helical configuration is much larger than that in the tokamak.

Keywords:

ray tracing, k_{\parallel} up-shift, fast wave current drive, electron heating

1. Introduction

It is an interesting subject to control Magneto-Hydro-Dynamics (MHD) stability by driving non-inductive current on the Large Helical Device (LHD) [1]. We have designed and developed an antenna called “comblin antenna” for a use in current drive and plasma heating (see Fig. 1 (a)) [2,3]. It is known that parallel refractive index (N_{\parallel}) affects the electron heating strongly. Fig. 2 shows a power deposition profile obtained from a simple calculation assuming the fixed parallel refractive index and the uniform RF electric field over the whole plasma radius. The electron heating become substantial for $N_{\parallel} > 6$ as the electron temperature on the magnetic axis, $T_{e0} = 3\text{keV}$.

The comblin antenna has a frequency pass-band, from which one can choose an adequate frequency and associated N_{\parallel} to optimize the current drive. However, if the wave N_{\parallel} -value changes itself as the wave travels, the prediction of the deposition profile may become quite different. Therefore, we employ the ray tracing analysis in this paper and try to give more accurate assessment of current drive by using the comblin antenna in LHD. This antenna can be used optionally in the second harmonic heating regime with higher magnetic field ($B_T = 2.75\text{ T}$, B_T is toroidal magnetic field). Under such condition, electron heating and ion heating are expected to be in competition. The ray tracing calculation allows an

assessment on the competition. LHD has loop antennas that have been used with frequency of 38.47 MHz (see Fig. 1 (b)). This paper gives also an assessment of this loop antenna on electron heating in the fundamental- and second harmonic-cyclotron frequency ranges.

2. Ray tracing method

We adopt the ray tracing method developed by McVEY [4] to investigate the wave propagation and the wave damping. The cold plasma dispersion relation was used in tracing the ray and the hot plasma dispersion relation was used in calculating the wave damping. With z-axis taken parallel to the magnetic field and with \mathbf{k} taken in x-z plane, the dispersion relation is given by Eq. (1).

$$G = \{(K_{xx} - N_z^2)(K_{yy} - N_x^2 - N_z^2) - K_{xy}K_{yx}\} \\ + \frac{K_{zx} + N_x N_z}{K_{zz} - N_x^2} \{K_{xy}K_{yz} - (K_{yy} - N_x^2 - N_z^2)(K_{xz} + N_x N_z)\} \\ + \frac{K_{zy}}{K_{zz} - N_x^2} \{K_{yx}(K_{xz} + N_x N_z) - K_{yz}(K_{xx} - N_z^2)\} = 0 \quad (1)$$

We use following definitions and approximations:

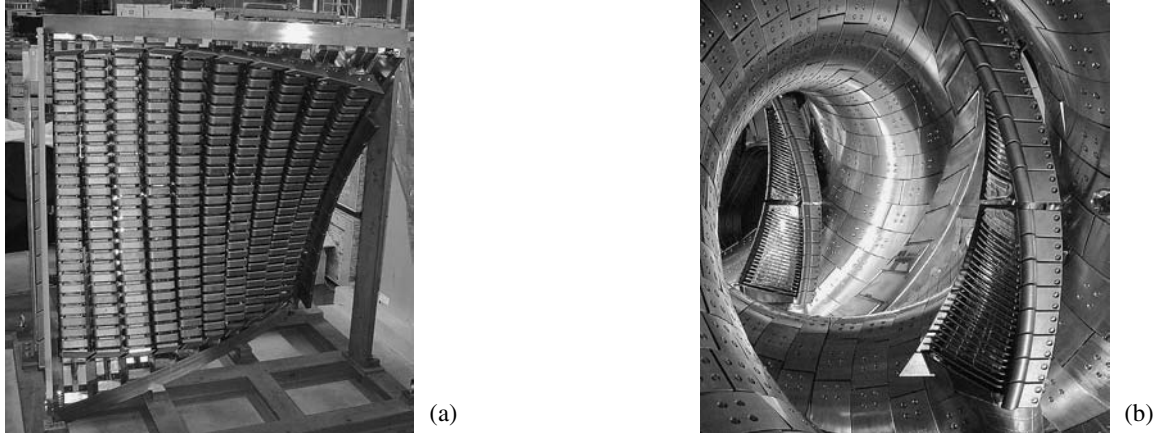


Fig. 1 Photos of ICRF antennas. (a) combine antenna (b) loop antenna.

$$K_{xx} \approx S_{stix}, K_{xy} \approx -K_{yx} \approx iD_{stix}, K_{zz} \approx P_{stix_e} \gg N_{\perp}^2,$$

$$K_{yz} \approx K_{zy} \approx 0, K_{zx} \approx K_{xz} \approx 0, \mu_0 = \frac{k_x^2 v_{te}^2}{2\omega_{pe}^2}, z_0 = \frac{\omega}{k_z v_{te}},$$

$$v_{te} = \sqrt{\frac{2T_e}{m_e}},$$

$$w(z) = \frac{1}{i\pi} \int_c dx \frac{\exp(-x^2)}{x-z}, \exp(-\mu_e) \approx 1,$$

$$\text{Re}[w(z_0)] \approx \exp(-z_0^2)$$

$$K_{zz} \approx P_{stix_e} \approx \frac{2\omega_{pe}^2 z_0^2}{\omega^2} [1 + i\sqrt{\pi} z_0 w(z_0)] = -\frac{\omega_{pe}^2 z_0^2}{\omega^2} Z'$$

to obtain

$$\text{Re}[G] \approx (S_{stix} - N_{\parallel}^2)(S_{stix} - N^2) - D_{stix}^2 = 0 \quad (2)$$

$$\text{Im}[G_{ion}] \approx \text{Im}[(K_{xx} - N_{\parallel}^2)(K_{xx} - N^2) + K_{xy}^2] \quad (3)$$

$$\text{Im}[G_{electron}] = \text{Im}[G_{Landau}] + \text{Im}[G_{TTMP}] \quad (4)$$

$$\text{Im}[G_{Landau}] \approx \frac{-N_{\parallel}^2 N_{\perp}^2 (S_{stix} - N_{\parallel}^2 - N_{\perp}^2)}{|Z'|^2}$$

$$\times \frac{\omega^2}{\omega_{pe}^2 z_0} 2\sqrt{\pi} \exp(-z_0^2)$$

$$\text{Im}[G_{TTMP}] \approx -\frac{1}{2} \sqrt{\pi} z_0 \beta_e N_{\perp}^2 (S_{stix} - N_{\parallel}^2) \exp(-z_0^2).$$

Here, S_{stix} , P_{stix} , D_{stix} are Stix's notations [5]. ω_{pe} is an electron plasma frequency. Z is a plasma dispersion function. β_e is beta value of electron. $\text{Re}[G]$ is the cold approximation of the real part of Eq. (1), $\text{Im}[G_{ion}]$, $\text{Im}[G_{Landau}]$, and $\text{Im}[G_{TTMP}]$ are the imaginary parts of Eq. (1) associated with ion cyclotron damping, electron Landau damping, and transit-time magnetic pumping (TTMP), respectively. The position and the wave number of the wave is obtained by integrating the equations

$$\frac{d\vec{r}}{dt} = -\frac{\partial \text{Re}[G]}{\partial \vec{k}} \Big/ \frac{\partial \text{Re}[G]}{\partial \omega}, \frac{d\vec{k}}{dt} = \frac{\partial \text{Re}[G]}{\partial \vec{r}} \Big/ \frac{\partial \text{Re}[G]}{\partial \omega} \quad (5)$$

and the wave energy E/E_0 is calculated by

$$E/E_0 = \exp\left(-2 \int (\text{Im}[G_{ion}] + \text{Im}[G_{electron}]) \Big/ \frac{\partial \text{Re}[G]}{\partial \omega} dt\right). \quad (6)$$

Within the parameter range of this paper, we find $k^{-3}(\partial k^2/\partial r) < 0.1$ and the validity of WKB is ensured.

3. Parameters used in the calculation

The following parameters were used in the calculation: the magnetic axis $R_{ax} = 3.6$ m, the density profile of $n_e = n_{e0}(1 - \rho^8)$ with $n_{e0} = 2.0 \times 10^{19} \text{ m}^{-3}$, and the temperature profile of $T = T_0(1 - \rho^2)$ with $T_0 = T_{e0} = T_{i0} = 3.0$ keV. Here, ρ is the normalized minor radius. The plasma consists of electrons and hydrogen ions.

The calculations were made for the four cases with following sets of parameters: (a) $f = 75.0$ MHz, $B_T = 1.5$ T, $k_{\parallel} = 13.9 \text{ m}^{-1}$ ($N_{\parallel} = 8.8$), (b) $f = 75.0$ MHz, $B_T = 2.75$ T, $k_{\parallel} = 13.9 \text{ m}^{-1}$ ($N_{\parallel} = 8.8$), (c) $f = 38.47$ MHz, $B_T = 1.5$ T, $k_{\parallel} = 5.0 \text{ m}^{-1}$ ($N_{\parallel} = 6.2$), and (d) $f = 38.47$ MHz, $B_T = 2.75$ T, $k_{\parallel} = 5.0 \text{ m}^{-1}$ ($N_{\parallel} = 8.8$).

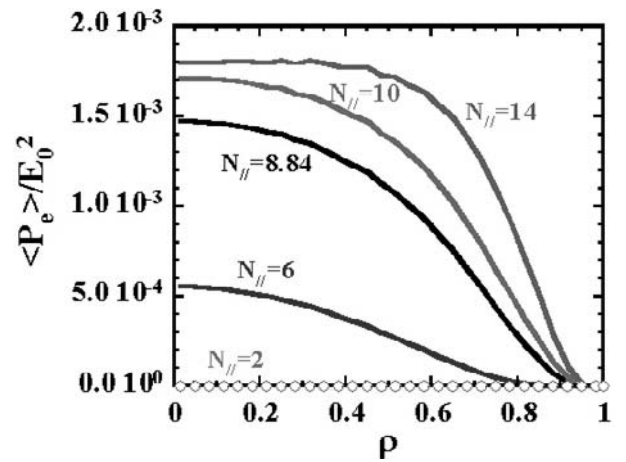


Fig. 2 Power deposition profile with fixed N_{\parallel} value over the whole plasma radius under uniform RF electric field ($|E_x|^2 + |E_y|^2 + |E_z|^2 = \text{const}$), the magnetic axis $R_{ax} = 3.6$ m, the density profile of $n_e = n_{e0}(1 - \rho^8)$ with $n_{e0} = 2.0 \times 10^{19} \text{ m}^{-3}$, the temperature profile of $T = T_0(1 - \rho^2)$ with $T_{e0} = T_{i0} = 3.0$ keV and hydrogen gas.

6.2), where B_T is magnetic field on magnetic axis and k_{\parallel} is parallel wave number at the ray tracing start point. Layers of the fundamental and the harmonics of ion cyclotron resonance and magnetic surfaces are shown with loop antennas in Fig. 3. In cases (a) and (b), the frequency is 75.0 MHz simulating the experiments using the combline antenna. In the case (a), ion cyclotron resonance layers of low harmonic number are excluded in favor of the electron heating and only the third and fourth harmonic resonance layer remains in the plasma. In case (b), a higher magnetic field is employed to locate second harmonic layer inside the plasma so that ion heating can take place. In cases (c) and (d), the frequency is 38.47 MHz simulating the experiments using the loop antenna. In case (c), the second harmonic layer is located inside the plasma. Thus, from the point of view of the wave absorption, cases of (b) and (c) are supposed to have the similar physical process. In case (d), the fundamental ion cyclotron resonance layer is located inside the plasma.

4. The results of the tray tracing calculations

The results of the calculations are shown in Fig. 4(a-d) corresponding to the cases (a-d), respectively. The boundary layer shown by thick solid line shows the Last Closed Flux Surface (LCFS). The fast wave propagates inside the R-cutoff layer, which has a shape of helically twisted ellipse locating a little inside the LCFS. The sharp turns of the ray appearing in these figures occur due to the reflection of the

wave at the cutoff layer with the complex geometry.

The figures consist of the top view of the typical ray trajectory shown in the left column and the partition of the power shown in the right column, where “s” on the abscissa is distance along the ray and R is the major radius. In Fig. 4(a), we find that electron damping is stronger than ion damping. It is noted that TTMP is a little larger than Landau damping in the considered plasma range. In Fig. 4(b), where $f = 75$ MHz and $N_{\parallel} = 8.8$, ion damping dominates over the electron damping due to the presence of the second harmonic layer. It is concluded that cyclotron layers of low harmonic numbers has to be avoided and a large $N_{\parallel} (= 8.8)$ has to be chosen in order to heat electrons and drive current.

In Fig. 4(c), where $f = 38.47$ MHz and $N_{\parallel} = 6.2$, the wave energy is absorbed by ions similarly to the case of 4(b); since the magnetic field was proportionally lowered, the second harmonic ion cyclotron resonance stays at the same place. The discontinuity of the curve in Fig. 4(c) is specifically large. It occurs due to the strong absorption of the wave as the ray meets the second harmonic layer by chance with low number of N_{\parallel} . It may be attributed to the factor $1/k_{\parallel}v_{th}$ in the imaginary part of the dispersion relation. The validity of the approximation separating the real and imaginary part may be lost there. However, it seldom occurs and if an average is taken over initial condition of k_{\parallel} and starting point, the estimation of the power fraction is affected little.

In Fig. 4(d), the ion damping is even stronger due to the presence of fundamental cyclotron layer.

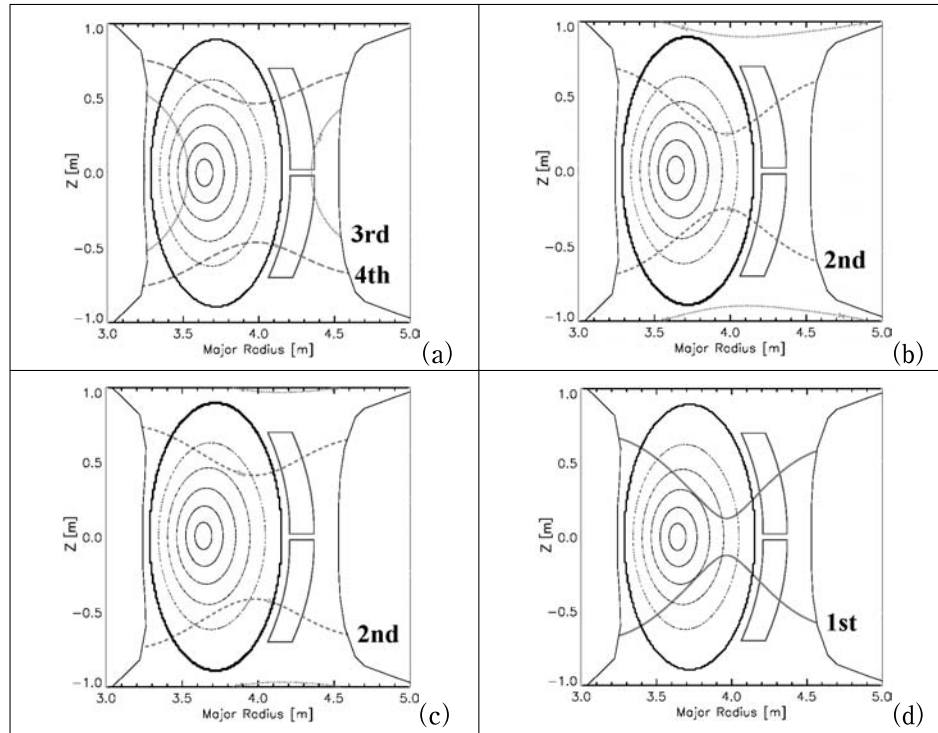


Fig. 3 Locations of ion cyclotron resonance layers, loop antenna, and contour line of flux surface; (a) $f = 75.0$ MHz, $B_T = 1.5$ T, $k = 13.9$ m $^{-1}$, (b) $f = 75.0$ MHz, $B_T = 2.75$ T, $k = 13.9$ m $^{-1}$, (c) $f = 38.47$ MHz, $B_T = 1.5$ T, $k = 5.0$ m $^{-1}$, (d) $f = 38.47$ MHz, $B_T = 2.75$ T, $k = 5.0$ m $^{-1}$. The notation of “1st”, “2nd”, “3rd” and “4th” show the fundamental ion cyclotron resonance layer, second harmonic resonance layer, third harmonic resonance layer and fourth harmonic resonance layer, respectively.

As it was reviewed preliminarily in section-1, the wave absorption by electrons is higher with larger value of N_{\parallel} (see Fig. 2). This feature was confirmed in the ray tracing analyses. However, the N_{\parallel} is not dependent only on its initial value. It was found in the calculation that the wave k_{\parallel} changed its values as the wave propagated in the torus. As k_{\parallel} affects the strength of the electron damping strongly, this

aspect is important.

In order to investigate the mechanism of the k_{\parallel} up-shift, the ray tracing was examined, for comparison, in the tokamak model magnetic field [6]

$$B_p(r) = \frac{B_0 a^2}{r q_a (R_0 + r \cos \theta)} \left[1 - \left(1 - \frac{r^2}{a^2} \right)^{q_a} \right], \quad (7)$$

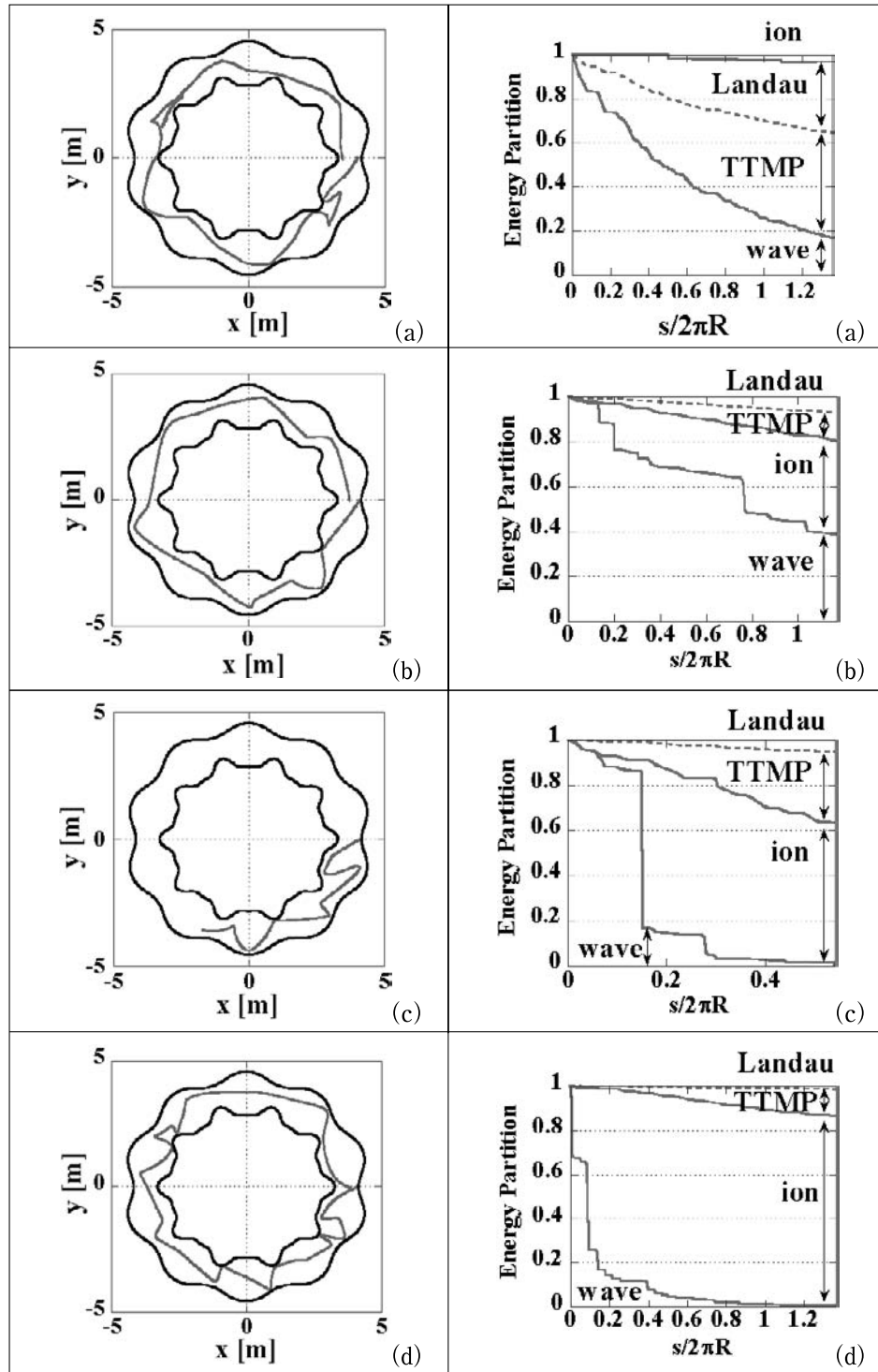


Fig. 4 Top view of the typical ray trajectory (left column) and the partition of the energy (right column), in which (a)-(d) correspond to the cases (a)-(d) in Fig. 3, respectively. The power absorbed by electrons are separated into those of electron Landau damping and TTMP.

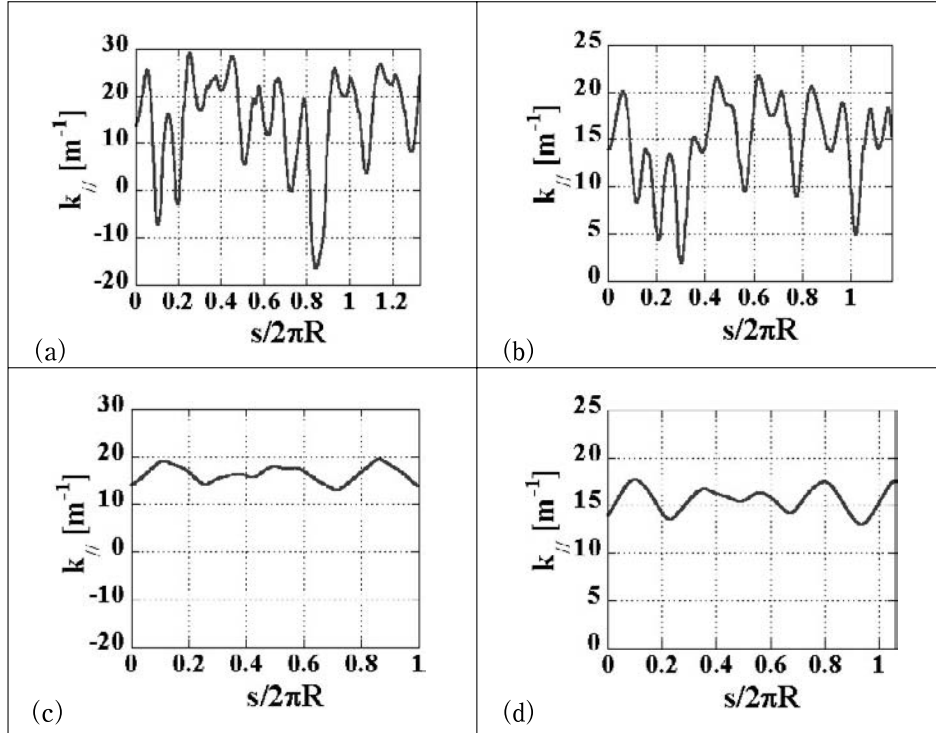


Fig. 5 k_{\parallel} versus the path length of the ray; (a) helical with $B_T = 1.5$ T, (b) helical with $B_T = 2.75$ T, (c) tokamak with $B_T = 1.5$ T and (d) tokamak with $B_T = 2.75$ T

where B_p is poloidal magnetic field and B_0 is toroidal magnetic field. R_0 is major radius and “ a ” is minor radius. θ is poloidal angle and q_a is safety factor at $r = a$.

Figure 5(a) and 5(b) show the k_{\parallel} versus the path length of the ray normalized to $2\pi R$, which is calculated for the helical configuration with $B_T = 1.5$ T and 2.75 T, respectively. Figure 5(c) and 5(d) are those calculated for the tokamak configuration with $B_T = 1.5$ T and 2.75 T, respectively. The k_{\parallel} -shift of the helical configuration (including up-shift and down-shift) was found much larger than that of the tokamak configuration. This may be attributed to the presence of stronger ripple in the helical system and the loss of conservation of toroidal mode number, which is ensured in the wave propagation in tokamaks.

5. Summary

Ray tracing calculations were carried out for the planned four experimental regimes on LHD. In case (a), ($f = 75.0$ MHz, $k_{\parallel} = 13.9$ m $^{-1}$, $B_T = 1.5$ T, $N_{\parallel} = 8.8$; combline antenna), the electron damping was stronger than the ion damping. In case (b), ($f = 75.0$ MHz, $k_{\parallel} = 13.9$ m $^{-1}$, $B_T = 2.75$ T, $N_{\parallel} = 8.8$; combline antenna) the electron damping was weak with respect to the ion damping. In case (c), ($f = 38.47$ MHz, $k_{\parallel} = 5.0$ m $^{-1}$, $B_T = 1.5$ T, $N_{\parallel} = 6.2$; loop antenna) the second harmonic ion heating was dominant over the electron heating. In case (d), ($f = 38.47$ MHz, $k_{\parallel} = 5.0$ m $^{-1}$, $B_T = 2.75$ T, $N_{\parallel} = 6.2$; loop antenna), the fundamental ion heating was dominant.

In the ray tracing calculation, a remarkable shift of k_{\parallel} -value was observed. The similar ray tracing calculation was made for a tokamak configuration with similar size and plasma parameters. It was found that the k_{\parallel} -shift on the helical configuration was much larger than that of the tokamak configuration. The mixed presence of helical ripple and tokamak ripple probably causes the difference of k_{\parallel} -shift. The k_{\parallel} -shift seems to be inherent in the helical configuration and it may play an important role in the field of electron heating and current drive.

Acknowledgments

This work was supported by JSPS-CAS Core-University Program on Plasma and Nuclear Fusion. The authors would like to thank the members of ICRF heating group at National Institute for Fusion Science, for their helpful comment and their support of calculations.

Reference

- [1] K. Ichiguchi *et al.*, Nucl. Fusion **33**, 481 (1993).
- [2] N. Takeuchi *et al.*, J. Plasma Fusion Res. SERIES **5**, 314 (2002).
- [3] Y. Takase *et al.*, Nucl. Fusion **44**, 296 (2004).
- [4] B.D. McVEY, Nucl. Fusion **19**, 461 (1979).
- [5] T.H. Stix, WAVES IN PLASMA (AIP, 1992) P7.
- [6] K.-L. Wong and M. Ono, Nucl. Fusion **23**, 805 (1983).